Lead-207 NMR Spectroscopic Study of Lead-Based Electronic Materials and Related Lead Oxides

Peidong Zhao, Subramanian Prasad, Jiong Huang, John J. Fitzgerald,* and Jay S. Shore*

Department of Chemistry and Biochemistry, South Dakota State University, Brookings, South Dakota 57007

Received: June 25, 1999

Static and MAS ^{207}Pb NMR spectra of a series of lead oxides, including the electronic materials $PbTiO_3$ (PT), $PbZrO_3$, $Pb(Zr_{0.53}Ti_{0.47})O_3$, $Pb(Mg_{0.33}Nb_{0.67})O_3$ (PMN), and 0.66PMN/0.34PT, have been measured. The chemical shift parameters (δ_{iso}, δ_{aniso}, and η) and the spin−lattice relaxation times have been determined for most of these compounds. The symmetry of the local environment of the lead(II) site and the covalency of the Pb−O bonds are determined to be the best indicators of the ^{207}Pb chemical shift parameters. Ionic compounds (e.g., $PbSO_4$ and $Pb(NO_3)_2$) have isotropic chemical shifts from −3600 to −2500 ppm and small absolute anisotropic chemical shifts (<500 ppm); while covalent lead oxides (e.g., PbO and Pb_3O_4) have isotropic chemical shifts from 800 to 1900 ppm and large absolute anisotropic chemical shifts (1900 to 2600 ppm). $PbTiO_3$ and $PbZrO_3$ have intermediate isotropic (−1419 to −1017 ppm) and anisotropic chemical shifts (−838 to −546 ppm) consistent with an intermediate degree of covalent bonding. $Pb(Zr_{0.53}Ti_{0.47})O_3$, PMN, and 0.66PMN/0.34PT have single broad asymmetric ^{207}Pb NMR resonances, with chemical shifts and line widths consistent with Pb−O bonds that are less covalent than those in PbO and more covalent than those in $PbTiO_3$ and $PbZrO_3$. For the ^{207}Pb NMR spectra of $Pb(Zr_{0.53}Ti_{0.47})O_3$, PMN, and 0.66PMN/0.34PT, chemical shift dispersion is a significant contribution to the line width, consistent with the presence of a range of inequivalent lead(II) sites in these disordered perovskite materials.

Introduction

Lead-containing materials are used in many applications despite the established chronic toxicity of many lead compounds. Lead-containing glasses have high refractive indices and are used in optical and electronic applications. PbS, PbTe, and PbSe are narrow band gap semiconductors useful as infrared lasers and detectors. The high transition temperature superconductors $Pb_2Sr_{0.9}La_{1.1}Cu_2O_{6.1}$ and $BaPb_{1-x}(Sb/Bi)_xO_3$ have also attracted much attention. Lead-containing perovskites (e.g., $PbTiO_3$, $PbZrO_3$, $Pb(Zr_xTi_{1-x})O_3$, $Pb(Mg_{0.33}Nb_{0.67})O_3$, and (1-*x*)$Pb(Mg_{0.33}Nb_{0.67})O_3$-*x*$PbTiO_3$ solid solutions) have extensive applications in the electronics industry due to their piezoelectric and ferroelectric properties and are used in capacitors, actuators, and sensors.[1−3] Solid-state ^{207}Pb NMR spectroscopy is an attractive technique to study the structure and bonding in these technologically important materials although a large chemical shift range, poor signal-to-noise ratio due to low natural abundance (22.6%), typically long relaxation times, and broad line shapes make solid-state ^{207}Pb NMR spectroscopy challenging.

The narrow band gap semiconductors, PbS, PbTe, and PbSe have been studied using solid-state ^{207}Pb NMR spectroscopy;[4−6] their carrier concentration has been related to the ^{207}Pb Knight shift.[4,5] An increase in the PbO composition in lead borosilicate glasses has been reported to be accompanied by an increase in the covalency of Pb−O bonds based on ^{207}Pb chemical shifts.[7,8] The metallic character of the PbO layers of several lead-containing cuprate superconductors has been determined from variable temperature ^{207}Pb NMR relaxation rate and Knight shift measurements.[9−12] The ferroelectric phase transition in $PbHPO_4$ was determined to be of the order−disorder type and mean-field-like from the temperature dependence of the ^{207}Pb chemical shift tensors.[13]

Recently, Neue et al. introduced a technique to measure broad NMR line shapes of static samples free from acoustic ringing and developed simulation software that accounted for other spectral distortions.[14] Neue et al. have measured the ^{207}Pb NMR spectra of α-PbO, *β*-PbO, $PbSO_4$, $Pb(NO_3)_2$, $PbCO_3$, $PbCrO_4$, $PbMoO_4$, $PbTiO_3$, $PbZrO_3$, $Pb(SCN)_2$, PbS, PbF_2, $PbCl_2$, $PbBr_2$, PbI_2, PbOHCl, PbOHBr, and PbOHI and determined the chemical shift parameters for the lead(II) sites in these compounds.[15−17] While the technique of Neue et al. does enable the measurement of broad NMR line shapes free from acoustic ringing, it is limited to line shapes narrower than approximately 500 kHz due to a limited excitation bandwidth.

Using static and MAS NMR spectroscopy, Fayon et al.[18] measured the chemical shift parameters (δ_{iso}, δ_{aniso}, and η) of the lead(II) sites in $PbSO_4$, $Pb(NO_3)_2$, $PbCO_3$, $PbMoO_4$, Pb_3O_4, PbO(yellow), PbO(red), $Pb_3(PO_4)_2$, $PbCl_2$, PbF_2, $PbSiO_3$, and H−Pb_2SiO_4. For ionic materials, the isotropic chemical shifts were observed to be correlated with the coordination number and mean Pb−O bond length.[18] For covalent compounds, the ^{207}Pb isotropic chemical shift had the strongest correlation with oxygen hybridization and the electronegativity of the second-nearest neighbor.[18]

Currently, there is intense interest in ferroelectric and piezoelectric lead-based materials, such as $PbTiO_3$, $PbZrO_3$, $Pb(Zr_xTi_{1-x})O_3$ (PZT), $Pb(Mg_{0.33}Nb_{0.67})O_3$ (PMN), and (1-*x*)$Pb(Mg_{0.33}Nb_{0.67})O_3$/*x*$PbTiO_3$ (PMN/PT) solid solutions.[1−3] PZT is used as a piezoelectric transducer. PMN and PMN/PT are used as electrostrictive actuators. While there is an incomplete understanding of their atomic-level behavior,[1,2,19−21] recent

* To whom correspondence should be addressed.

10.1021/jp992162r CCC: $18.00
Published on Web 11/12/1999

TABLE 1: Important Structural Parameters of Lead Sites in Various Lead Oxides

compound	nearest-neighbor oxygen[a]	symmetry of unit cell	Pb−O distances (Å)	avg. Pb−O distance	ref.
$PbSO_4$	12	orthorhombic	2.55, 2.60(2), 2.66, 2.76(2), 2.98(2), 3.06(2), 3.22(2)	2.87	52
$Pb(NO_3)_2$	12	cubic	2.75(6), 2.87(6)	2.81	51
$PbNb_2O_6$					
site 1	12	trigonal	2.34(3), 2.55(3), 3.01(6)	2.45	29
site 2	6		2.55(3), 2.60(3)	2.58	
site 3	6		2.57(3), 3.35(3)	2.96	
$PbCO_3$	9	orthorhombic	2.59, 2.62(2), 2.72(2), 2.75(2), 2.78(2)	2.70	57
$PbCrO_4$	13	orthorhombic	2.66, 2.70(2), 2.76(2), 2.87, 2.93(2), 2.97(2), 3.44(2), 3.50	2.97	52, 72
$PbWO_4$	8	tetragonal	2.591(4), 2.601(4)	2.60	52
$PbMoO_4$	8	tetragonal	2.491(4), 2.823(4)	2.66	52
PbC_2O_4	7	triclinic	2.43, 2.45, 2.49, 2.61, 2.65, 2.84, 2.90	2.64	54
$PbTiO_3$	12	tetragonal	2.53(4), 2.80(4), 3.20(4)	2.84	50, 57, 58
$PbZrO_3$					
site 1	12	orthorhombic	{2.53, 2.58, 2.59, 2.66, 2.82(2), 2.91, 3.07, 3.27, 3.30, 3.33, 3.57}	2.95	50, 57, 59−61
site 2	12		{2.26, 2.58, 2.59, 2.66, 2.82, 3.07(2), 3.13, 3.27, 3.30, 3.33, 3.36}	2.95	
Pb_3O_4					
Pb(IV)	6	tetragonal	2.13(2), 2.14(4)	2.14	50, 56, 57
Pb(II)	4		2.13, 2.18(2), 3.01	2.38	
PbO(yellow)	4	orthorhombic	2.20(2), 2.49(2)	2.35	50, 55
PbO(red)	4	tetragonal	2.30(4)	2.30	50, 55
$Pb(Zr_{0.53}Ti_{0.47})O_3$	12	tetragonal	2.60 to 3.32		65−68
$Pb(Mg_{0.33}Nb_{0.67})O_3$	12	pseudo-cubic	2.48 to 3.25		69, 70
0.66PMN/0.34PT	12	rhombohedral	unknown		

[a] Oxygen within 3.5 Å of the lead are defined as nearest-neighbor oxygen.

EPR investigations have suggested that the covalency of the Pb−O bonds is important to the ferroelectric and piezoelectric properties of these materials.[22] In the work reported here, static and MAS ^{207}Pb NMR spectra of several lead salts, lead oxides, $PbTiO_3$, $PbZrO_3$, $Pb(Zr_{0.53}Ti_{0.47})O_3$, PMN, and 0.66PMN/0.34PT have been measured. The ^{207}Pb chemical shift parameters (δ_{iso}, δ_{aniso}, and η) of these compounds are interpreted in terms of the symmetry of the lead(II) environments and the covalency of the Pb−O bonds; these structural parameters were determined to be the best indicators of the ^{207}Pb chemical shift parameters and not the coordination number and average Pb−O bond lengths as had been concluded by Fayon et al.[18] The correlation between the symmetry of the lead(II) environment and isotropic and anisotropic chemical shifts is used here to assign ^{207}Pb NMR resonances to specific crystallographic sites in $PbZrO_3$ and $PbNb_2O_6$.

Experimental Section

$PbNb_2O_6$, $Pb(Zr_{0.53}Ti_{0.47})O_3$, PMN, and 0.66PMN/0.34PT were synthesized as described in the literature; their purity was verified using powder X-ray diffraction.[23−26] All of the other samples used in this study were obtained from Alfa Aesar (Ward Hill, MA) or Aldrich Chemical Co. Inc. (Milwaukee, WI) with a stated purity of 98% or higher. $PbNb_2O_6$ was synthesized by mixing PbO and Nb_2O_5 in a ratio corresponding to the formula in ethanol for 1.5 h. The paste was then dried in an oven (140 °C) overnight and then fired at 1000 °C for 4 h.[27,28] While there are two structural forms of $PbNb_2O_6$,[2] the nonferroelectric rhombohedral structural form, as obtained by firing below 1250 °C, was studied here; the ferroelectric orthorhombic form can be obtained by firing above 1250 °C.[28,29] The lead zirconate titanate, $Pb(Zr_{0.53}Ti_{0.47})O_3$, was prepared by mixing PbO, ZrO_2, and TiO_2(anatase) in ethanol for 2 h, followed by drying at 110 °C, and firing at 900 °C. PMN was synthesized by modifying the columbite method.[30] The columbite precursor ($MgNb_2O_6$) was prepared by mixing Nb_2O_5 with a 2% excess of $(MgCO_3)_4$-$Mg(OH)_2 \cdot 5H_2O$ in ethanol for 2 h, followed by drying the paste at 140 °C overnight, and then firing at 1000 °C for 6 h. The $MgNb_2O_6$ precursor was mixed with PbO according to the PMN formula in ethanol for 1.5 h, followed by a two-stage firing at 800 °C for 2 h, and then at 900 °C for 2 h following the procedure of Gupta and Kulkarni.[1] The 0.66PMN/0.34PT powder was synthesized by mixing the PMN powder prepared from the modified columbite method with TiO_2 (anatase) (Aldrich, 99.9+%) and PbO (Alpha, 99.9995%, 0.5% excess). The powder mixture was ground for 1 h in ethanol, solvent dried in an oven (140 °C) overnight, and then calcined at 900 °C for 4 h.

The ^{207}Pb NMR spectra were measured at 4.7 T (^{207}Pb: 46.86 MHz) or 9.4 T (^{207}Pb: 83.72 MHz) using a Chemagnetics-200 or Bruker ASX-400 spectrometer, respectively. A Chemagnetics MAS probe and 7 mm rotors were used to acquire spectra at 4.7 T. A "home-built" NMR probe and a Bruker MAS probe with 4 mm rotors were used to acquire static and MAS spectra at 9.4 T, respectively. A Hahn spin−echo pulse sequence was used to acquire both static and MAS spectra. For the MAS spectra, the delay between 90° and 180° pulses was set to an integral multiple of the rotor period. The recycle delays were optimized for signal-to-noise and were typically between 20 and 50 s. ^{207}Pb chemical shifts are reported with respect to tetramethyl lead in toluene using 1.0 M $Pb(NO_3)_2$(aq) (−2961 ppm) as an external secondary standard.[16] The chemical shifts were converted from Hertz to ppm by dividing by the frequency of tetramethyl lead in toluene. All NMR spectra were processed using the computer program RMN[31] and were apodized with 100−300 Hz Lorentzian or 20−500 Hz Gaussian line broaden-

TABLE 2: Measured ^{207}Pb NMR Parameters

compound	T_1 (s)	T_2 (ms)	δ_{iso} (ppm)[a]	δ_{aniso} (ppm)[a]	η	MAS fwhh (kHz)
$PbSO_4$	10.2		−3611	−317	0.6	0.1
$Pb(NO_3)_2$	8.0		−3494	−36	0.0	0.05
$PbNb_2O_6$						
site 1	30	1.7	134	−2024	0.0	2.0
site 2 and 3	5.6		−2829	149	0.0	1.8
$PbCO_3$ (ref 62)			−2641	−456	0.4	
$PbCrO_4$ (ref 62)			−2292	457	0.9	
$PbWO_4$ (ref 62)			−2003	135	0.0	
$PbMoO_4$ (ref 63)			−1989	126	0.0	
PbC_2O_4	20.4		−1642	−1083	0.2	1.8
$PbTiO_3$	7.1		−1419	−772	0.0	2.0
$PbZrO_3$						
site 1	4.2		−1363	−546	0.2	3.0
site 2	5.5		−1017	−838	0.2	3.0
Pb_3O_4						
Pb(IV)	44		−1101	98	0.0	1.0
Pb(II)	160		808	−1910	0.3	4.1
PbO(yellow)	24.8	0.74	1536	−2576	0.1	3.2
PbO(red)	1.5	0.44	1878	−2212	0.0	2.0
$Pb(Zr_{0.53}Ti_{0.47})O_3$	7.3					
$Pb(Mg_{0.33}Nb_{0.67})O_3$	1.0	0.2				
0.66PMN/0.34PT	4.6					

[a] All chemical shift parameters are relative to 1.0 M $Pb(NO_3)_2$ observed at −2961 ppm.

ing before Fourier transformation of MAS or static spectra, respectively. The chemical shift parameters (Table 2) were determined by fitting static and MAS spectra to simulated line shapes using a computer program written in the C/C^{++} language which included a conjugate gradient chi-squared minimization algorithm. The subroutine used to simulate the MAS line shapes is based on the Herzfeld−Berger analysis of spinning sideband patterns.[32,33] In Figure 1, experimental and simulated, static and MAS spectra of $PbSO_4$ are shown. For those compounds with relatively large anisotropic chemical shifts (e.g., $PbZrO_3$ and $PbTiO_3$), the spectra measured at 4.7 T were used to determine the chemical shift parameters. The uncertainties in the NMR parameters as determined by comparison of MAS and static spectra measured at multiple field strengths are estimated to be ±5 ppm for δ_{iso}, ± 3% for δ_{aniso}, and ±0.1 for η.

Broad ^{207}Pb NMR resonances (full width at half-height > 80 kHz) were measured using a "point-by-point" method. A single free induction decay was measured at a frequency; the frequency offset was then incremented by 10 kHz. This was typically done thirteen times corresponding to a sweep width of 130 kHz. The frequency offset was then set to the original value, and the process was repeated until sufficient signal-to-noise was acquired (typically 500 cycles). The time between acquisition of free-induction decays was one-thirteenth of the normal recycle delay, greatly reducing the time required to measure such broad line shapes. The NMR probe was tuned every 100 kHz. Low power pulses were used to excite only small bandwidths (8 kHz). Considering the distance in frequency between data points and using simple propagation of error calculations, the uncertainty in the NMR parameters determined from the "point-by-point" spectra are estimated to be ±35 ppm for δ_{iso}, ±70 ppm for δ_{aniso}, and less than ±0.1 for η, except for PbC_2O_4 which, due to the relatively small δ_{aniso}, the uncertainty in η is ±0.15.

Spin−lattice relaxation times (T_1) were measured using a saturation−recovery pulse sequence, and fitting the intensities to the equation $I(t) = I_o*(1 - \exp(-t/T_1))$, where I_o is the maximum observed intensity and $I(t)$ is the intensity corresponding to a recovery time of t. Theoretical curves were fit to the experimental data by varying I_o and T_1 and using a least-squares algorithm. A series of 90° pulses separated by a progressively decreasing increment of time was used to initially saturate the signal. Spin−spin relaxation times (T_2) were measured using a Hahn spin−echo pulse sequence and incrementing the time (τ) between the 90° and 180° pulses. The signal intensities were fit to the equation $I(\tau) = I_o*\exp(-\tau/T_2)$ by varying I_o and T_2. Both spin−lattice and spin−spin relaxation times were measured on static samples. For broad ^{207}Pb NMR resonances, the relaxation time of the highest intensity singularity of the line shape was measured. Both T_1 and T_2 values (Table 2) are accurate to within typically ±4%.

Theoretical Background

The chemical shift interaction typically dominates the line shape of solid-state ^{207}Pb NMR spectra. The homonuclear dipolar and scalar interactions are usually negligible due to the low natural abundance (22.6%) and relatively small gyromagnetic ratio ($\gamma = 5.540 \times 10^7$ radT^{-1} s^{-1}) of ^{207}Pb.[34] The chemical shielding interaction, which is dependent on the relative orientation between the crystal axis and the external magnetic field (B_o), is treated as a perturbation to the Zeeman interaction and can be written as

$$H_{cs} = \gamma\hbar\mathbf{I}\sigma B_o \tag{1}$$

where γ is the gyromagnetic ratio, **I** is the nuclear spin operator, and σ is the chemical shielding tensor. The three diagonal elements of the chemical shielding tensor defined as σ_{xx}, σ_{yy}, and σ_{zz} (units of Hz) are often expressed relative to a standard (e.g., tetramethyl lead in toluene) in terms of the chemical shifts δ_{xx}, δ_{yy}, and δ_{zz} (units of ppm), defined such that $|\delta_{zz} - \delta_{iso}| \geq |\delta_{yy} - \delta_{iso}| \geq |\delta_{xx} - \delta_{iso}|$. Using this formalism, the relationship between chemical shift and chemical shielding values is $\delta = 10^6 (\sigma_{std} - \sigma)$, where σ_{std} is the isotropic chemical shielding value of the standard. The isotropic chemical shift (δ_{iso}), anisotropic chemical shift (δ_{aniso}), and asymmetry parameter (η) can also be used to characterize the chemical shielding interaction and can be defined as

$$\delta_{iso} = \frac{\delta_{xx} + \delta_{yy} + \delta_{zz}}{3} \tag{2}$$

$$\delta_{aniso} = \delta_{zz} - \delta_{iso} \qquad \eta = \frac{\delta_{xx} + \delta_{yy}}{\delta_{zz} + \delta_{iso}} \tag{3}$$

Both the anisotropic chemical shift (δ_{aniso}) and the asymmetry parameter (η) are related to the symmetry of the electronic environment around the nucleus. The anisotropic chemical shift will be zero if the local environment around the nucleus has at least two non-collinear C_3 axes or has higher symmetry.[35] The chemical shift asymmetry parameter (η) will be zero when the local environment around the nucleus has a single C_3 (or higher) symmetry axis.

Due to the orientational dependence of the chemical shielding interaction, NMR spectra of powders consist of a distribution of NMR frequencies. Spinning a powder sample about 54.74° (the magic angle) relative to the external magnetic field (B_o), causes the anisotropic contribution to the line shape to be orientationally averaged and a high-resolution NMR spectrum can be measured.[36−38] The observed NMR spectra of both static and spinning powder samples can be fit to simulated line shapes to determine the chemical shift parameters.

For heavy atoms, such as lead, relativistic effects, such as spin−orbit coupling, are important to the chemical shielding

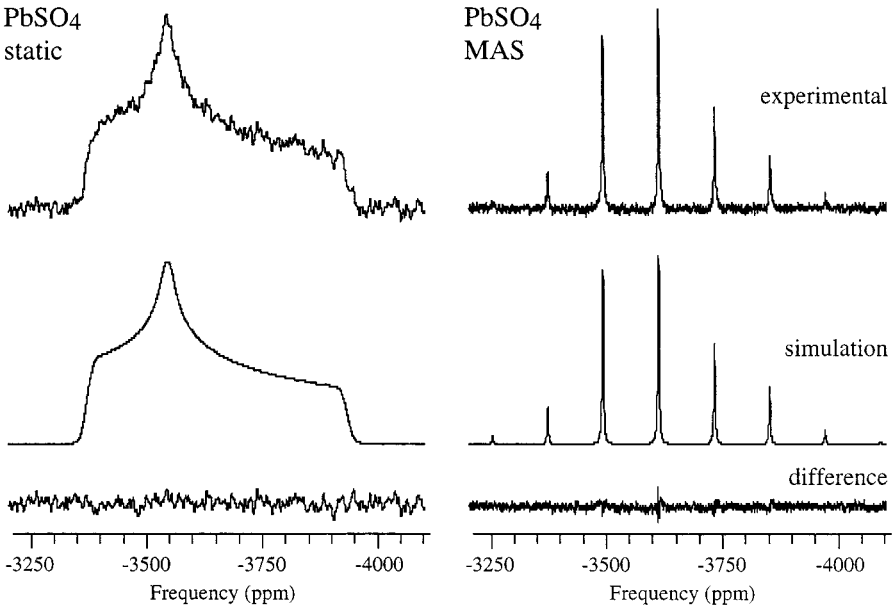

Figure 1. Experimental (top), simulated (middle), and difference (bottom) static and MAS ^{207}Pb NMR spectra of $PbSO_4$ measured at 4.7 T. The MAS spectrum of $PbSO_4$ was acquired with a spinning rate of 5.0 kHz.

interaction.[4,5,39−41] However, to illustrate the correlation between structure and the isotropic and anisotropic chemical shifts, only a simplistic description of the origins of the chemical shielding interaction is given here. The chemical shielding interaction originates from the interaction between the nuclear magnetic moment and the electron orbital angular momentum of the surrounding electrons, and consists of both diamagnetic and paramagnetic contributions.[42−47] The diamagnetic contribution results from a current being induced in the electron cloud by the external magnetic field producing a magnetic field (B_{loc}) at the nucleus that is proportional to and opposes the external magnetic field (B_o). Hence, the frequency needed for resonance is lowered. The diamagnetic contribution is dominated by core electrons due to its dependence on the distance between the electrons and the nucleus.

The paramagnetic contribution results from the partial alignment of the orbital angular momentum of the electron cloud with the external magnetic field and can be calculated using perturbation theory, treating the static magnetic field (B_o) and nuclear magnetic moments as perturbations and using the electronic wave functions from zero magnetic field.[42−47] For an atom or ion in a highly symmetric environment, the orbital angular momentum is quenched and there is no paramagnetic contribution. An asymmetric local electronic environment results in a mixing of excited states and an unquenching of the orbital angular momentum which results in a paramagnetic contribution to the chemical shift. The more asymmetric the local environment or the smaller the excited state energy, the larger the paramagnetic contribution. For heavy atoms and ions such as Pb(II), the energy difference between ground and excited states is relatively small due to the orbitals being in the same electron shell.

The paramagnetic contribution is dominated by outer shell electrons and hence is highly sensitive to the local atomic structure and bonding environment. For NMR spectra of heavy atoms and ions, the large ranges of isotropic and anisotropic chemical shifts are due to the paramagnetic contribution. Even though the isotropic and anisotropic chemical shifts are affected differently by the symmetry of the local electronic environment, a correlation between isotropic and anisotropic chemical shifts is expected for heavy atoms or ions with filled electronic subshells, such as ^{207}Pb(II) and ^{119}Sn(II).[47]

Results and Discussion

Static and MAS ^{207}Pb NMR spectra of a series of lead oxides, including the electronic materials $PbTiO_3$, $PbZrO_3$, $Pb(Zr_{0.53}Ti_{0.47})O_3$, PMN, and 0.66PMN/0.34PT were measured. The number of nearest-neighbor oxygen, the symmetry of the unit cell, the Pb−O distances, and the average Pb−O distance of the compounds studied and the corresponding literature references are given in Table 1. Accurate Pb−O distances for $Pb(Zr_{0.53}Ti_{0.47})O_3$, PMN, and 0.66PMN/0.34PT are not available due to the disordered nature of these materials. For all of the compounds studied, oxygen are the nearest atoms to lead. Hence, the number of nearest-neighbor oxygen and Pb−O distances can be used to characterize the local lead environment and should be related to the ^{207}Pb chemical shift parameters. In this work, oxygen within 3.5 Å of lead are defined as nearest-neighbor oxygen based on the van der Waals radii of oxygen (1.5 Å) and lead (2.0 Å).[48] Any atom within the sum of the van der Waals radii perturbs the local electronic environment enough to affect the NMR parameters. Using van der Waals radii to count nearest-neighbor oxygen to interpret ^{207}Pb NMR spectra is different than in previously reported studies.[18] The sum of the ionic radii of O^{2-} (1.40 Å) and Pb^{2+} (1.18 Å, for lead coordinated to six oxygen) is used in this study to qualitatively describe the degree of covalency of Pb−O bonds.[49]

^{207}Pb NMR Spectroscopy of Simple Lead Oxides. $PbSO_4$ and $Pb(NO_3)_2$ are known to be ionic compounds.[50] Experimental and simulated, static and MAS ^{207}Pb NMR spectra of $PbSO_4$ are shown in Figure 1. For $PbSO_4$ and $Pb(NO_3)_2$, all of the Pb−O distances are close to or larger than the sum of the Pb^{2+} and O^{2-} ionic radii (2.58 Å),[51,52] consistent with the small paramagnetic contribution to the isotropic chemical shifts and the relatively small anisotropic chemical shifts. The symmetry of the lead environment in lead nitrate is higher than that in lead sulfate,[51,52] consistent with the ^{207}Pb NMR resonance of $Pb(NO_3)_2$ having a smaller absolute anisotropic chemical shift (−36 ppm compared to −317 ppm).

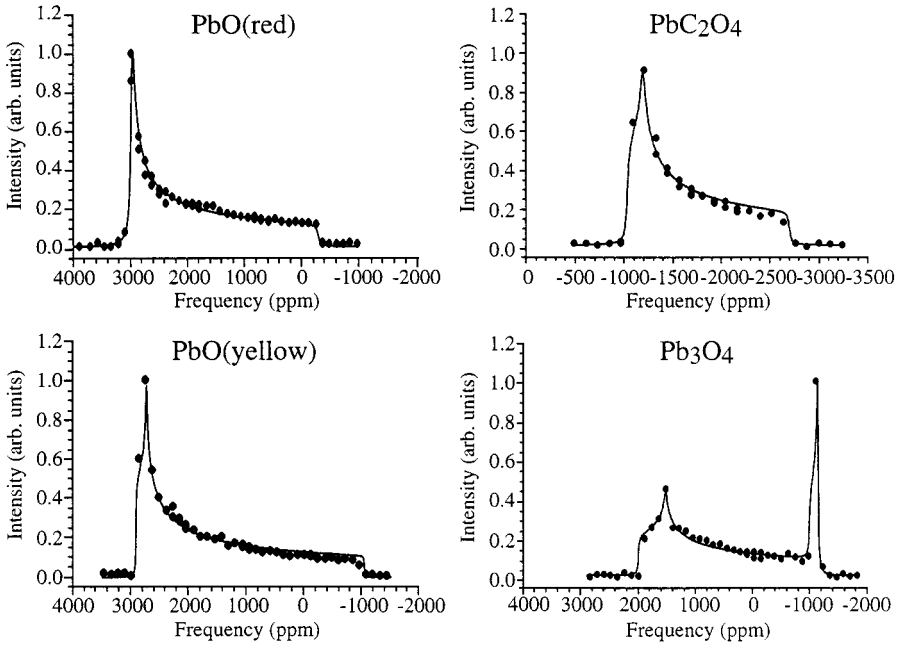

Figure 2. ^{207}Pb NMR spectra of PbO (red), PbO(yellow), PbC_2O_4, and Pb_3O_4 acquired at 9.4 T using the "point-by-point" method (see the Experimental Section for details). The filled circles are the measured intensities at each frequency. The solid lines are simulated line shapes fit to the data.

The ^{207}Pb NMR spectra of PbO (red), PbO (yellow), PbC_2O_4, and Pb_3O_4 acquired using the "point-by-point" method are shown in Figure 2. The lines are simulated line shapes fit to the experimental spectra. The point-by-point method was used because these spectra could not be measured accurately at 9.4 T using conventional NMR techniques due to their large breadths (140−330 kHz).

PbC_2O_4 is not an electronic material but is an important precursor for the synthesis of the piezoelectric material PMN by the oxalate chelation method.[53] The Pb(II) site in PbC_2O_4 has seven nearest-neighbor oxygen with Pb−O distances from 2.43 to 2.90 Å. The oxygen closest to the Pb(II) ion (2.43 Å, 2.46 Å, 2.49 Å) are on the same side, resulting in a very asymmetric local environment,[54] consistent with the observed isotropic (−1642 ppm) and anisotropic (−1083 ppm) chemical shifts, and nonzero asymmetric parameter ($\eta = 0.2$).

Lead monoxide (PbO) has two polymorphs, red (litharge) and yellow(massicot), with tetragonal and orthorhombic unit cell symmetries, respectively.[50,55] For PbO(red), the Pb(II) site has a square pyramidal electronic configuration (C_{4v} symmetry) with a lone pair of electrons at the apex and four equivalent Pb−O bonds 2.30 Å long.[50,55] The C_{4v} symmetry of this lead(II) site is consistent with the asymmetry parameter of zero ($\eta = 0.0$) determined from the experimental spectrum shown in Figure 2. The Pb(II) site in PbO(yellow) has two Pb−O bonds 2.20 Å long, another pair 2.49 Å long, and a lone pair of electrons at the apex of a distorted square pyramidal electronic configuration,[50,55] consistent with an asymmetry parameter of 0.1. From the static ^{207}Pb NMR spectra, both lead monoxides have very large anisotropic chemical shifts (−2212 and −2576 ppm) and paramagnetically shifted isotropic chemical shifts (1878 and 1536 ppm), consistent with the electron density of these Pb(II) sites being far from spherically symmetric in part due to the presence of a lone pair of electrons. The larger absolute anisotropic chemical shift of PbO (yellow) is consistent with the lower symmetry of its Pb(II) site.

The ^{207}Pb NMR spectrum of Pb_3O_4 shown in Figure 2 has two overlapping resonances due to a Pb(II) and a Pb(IV) site. The assignment of the NMR resonances to these two sites and the associated ^{207}Pb NMR parameters are summarized in Tables 1 and 2. The Pb(IV) site in Pb_3O_4 is in a pseudo-octahedral environment with six nearest-neighbor oxygen as shown in Figure 3.[50,56,57] The Pb(IV) site has a highly symmetric electronic environment and thus has a small paramagnetic contribution to the chemical shift and a 98 ppm anisotropic chemical shift (determined from a spectrum not shown). The Pb(II) site of Pb_3O_4 has four nearest-neighbor oxygen with three short Pb−O distances of 2.18, 2.18, and 2.13 Å. The fourth Pb−O distance is 3.01 Å. The asymmetric local electronic environment of this site is consistent with the paramagnetically shifted isotropic (808 ppm) and substantial anisotropic (−1910 ppm) chemical shifts.

The ^{207}Pb MAS NMR spectra of the Pb(IV) site in Pb_3O_4 measured at 4.7 and 9.4 T are shown in Figure 3. The observed spectra have a field-independent splitting of 2.3 kHz, which is due to *J* coupling between the Pb(IV) and Pb(II) sites. Due to the line widths of the peaks (4.1 kHz) in the MAS spectrum of the Pb(II) site (data not shown), no splitting was observed. The Pb(IV) site is surrounded by eight next nearest-neighbor Pb(II) ions. While there is only one Pb(IV) and one Pb(II) site, scalar coupling between the Pb(IV) and Pb(II) sites can occur via two separate pathways. For one pathway, two Pb(II) are connected to a Pb(IV) through a common oxygen; the other pathway consists of a bridging oxygen between a Pb(II) and two Pb(IV), as shown in Figure 3. The spectral intensities are consistent with the scalar coupling being between the Pb(IV) and only four of the surrounding Pb(II). While the scalar coupling in Pb_3O_4 has been previously reported, it was incorrectly attributed to coupling between Pb(IV) sites which are magnetically equivalent.[18]

Numerous mixed metal oxide systems such as the ferroelectric lead titanate ($PbTiO_3$) and lead zirconate ($PbZrO_3$) have the formula ABO_3 and a perovskite lattice structure. The structures of $PbTiO_3$ (cubic phase), $PbTiO_3$ (tetragonal phase), and $PbZrO_3$ (orthorhombic phase) are shown in Figure 4. In the perovskite structure, the A ions (e.g., Pb(II)) are in 12-coordinate AO_{12} sites, and the B ions (e.g., Ti(IV) and Zr(IV)) are in 6-coordinate BO_6 sites. Lead titanate undergoes a cubic to tetragonal phase transition as the temperature is reduced below 490 °C. Only the tetragonal form is ferroelectric. Its electrical properties are related to the displacement of the Ti(IV) and Pb(II) ions from

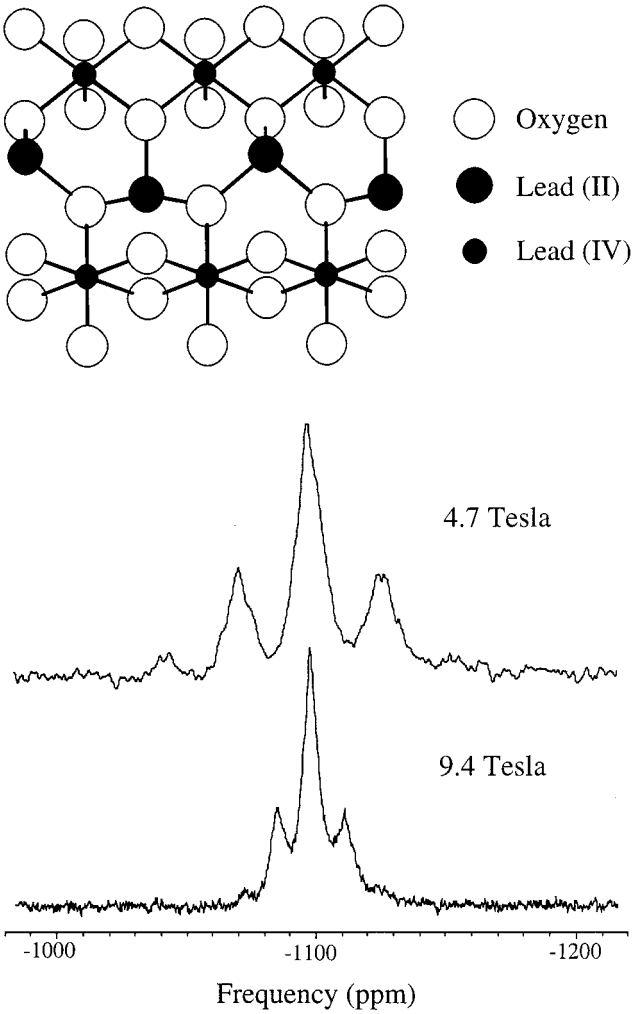

Figure 3. The structure of Pb_3O_4 and MAS ^{207}Pb NMR spectra of the Pb(IV) site in Pb_3O_4 acquired at 4.7 and 9.4 T. The field independent splitting observed in the NMR spectra is 2.3 kHz.

their ideal cubic positions by 0.30 and 0.47 Å, respectively.[2,58] Lead zirconate, in contrast, is an antiferroelectric material with orthorhombic unit cell symmetry below 230 °C.[2,59−61]

Static and MAS ^{207}Pb NMR spectra of lead titanate ($PbTiO_3$) and lead zirconate ($PbZrO_3$) are shown in Figure 5. From the spectra of $PbTiO_3$, an asymmetry parameter of zero ($\eta = 0.0$) was determined, consistent with $PbTiO_3$ having a single lead(II) site with C_{4v} symmetry. In lead titanate, twelve oxygen surround each lead(II) with four Pb−O distances of 2.53 Å, four of 2.80 Å, and four of 3.20 Å.[50,57,58] The covalency of the four short Pb−O bonds results in lower symmetry of the charge distribution around the lead(II), consistent with the observed isotropic ($\delta_{iso} = -1419$ ppm) and anisotropic ($\delta_{aniso} = -772$ ppm) chemical shifts.

The two lead(II) sites in $PbZrO_3$ are readily observed in the static ^{207}Pb NMR spectrum shown in Figure 5. Both Pb(II) sites have twelve nearest-neighbor oxygen and three Pb−O distances shorter than or approximately 2.58 Å (2.26 Å, 2.58, 2.59, and 2.53 Å, 2.58 Å, 2.59 Å),[50,57,59−61] consistent with the observed isotropic (−1017 and −1363 ppm) and anisotropic (−838 and −546 ppm) chemical shifts. The ^{207}Pb NMR resonance with the more paramagnetically shifted isotropic (−1017 ppm) and larger anisotropic (−838 ppm) chemical shift is assigned to the lead(II) site with the shortest Pb−O bond length (2.26 Å).

Interpretation of NMR-Measured Parameters of Simple Lead Oxides. The chemical shift parameters (δ_{iso}, δ_{aniso}, and

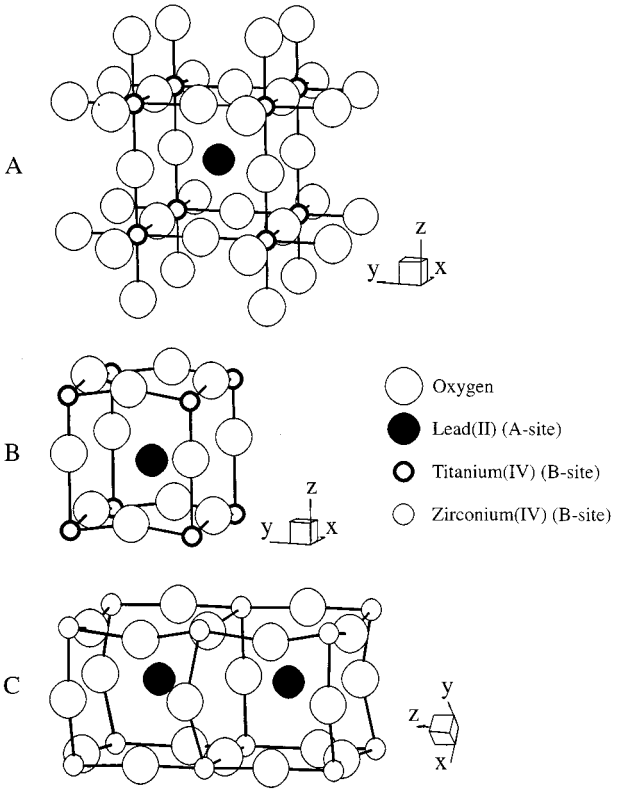

Figure 4. The structure of (A) $PbTiO_3$ (cubic phase), (B) $PbTiO_3$ (tetragonal phase), and (C) $PbZrO_3$ (orthorhombic phase). The two distinct Pb(II) sites in $PbZrO_3$ are shown.

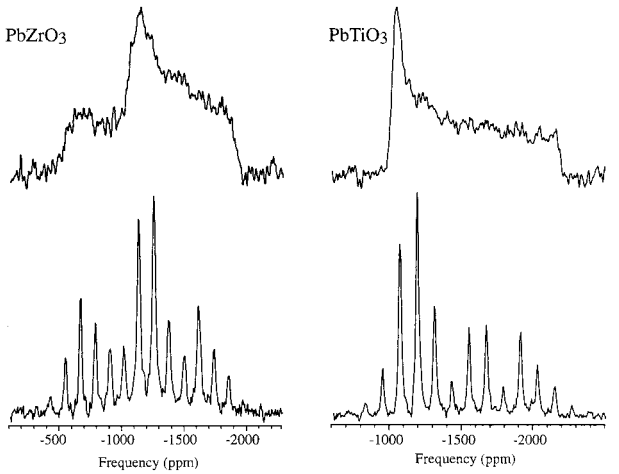

Figure 5. Static (top) and MAS (bottom) ^{207}Pb NMR spectra of $PbZrO_3$ and $PbTiO_3$. The MAS spectra were acquired at 9.4 T with a spinning rate of 10 kHz. The static spectra were acquired at 4.7 T.

η) determined by fitting MAS and static spectra to simulated line shapes, the full width at half-height (fwhh) of the peaks in MAS spectra, longitudinal relaxation times (T_1), and transverse relaxation times (T_2) for the lead oxide systems measured in this work ($PbSO_4$, $Pb(NO_3)_2$, $PbNb_2O_6$, PbC_2O_4, $PbTiO_3$, $PbZrO_3$, Pb_3O_4, PbO(yellow), PbO(red), $Pb(Zr_{0.53}Ti_{0.47})O_3$, $Pb(Mg_{0.33}Nb_{0.67})O_3$, and (0.66)PMN/(0.34)PT) are summarized in Table 2. The ^{207}Pb chemical shift parameters of $PbCO_3$, $PbCrO_4$, and $PbWO_4$ from Nolle[62] and of $PbMoO_4$ from Lauterbur and Burke[63] are also given in Table 2. The isotropic and anisotropic chemical shifts measured in this study are within 4 and 5 ppm, respectively, of the values reported by Neue et al.[16] for $Pb(NO_3)_2$ and those reported by Fayon et al.[18] for $PbSO_4$ and $Pb(NO_3)_2$. There are larger differences between our values

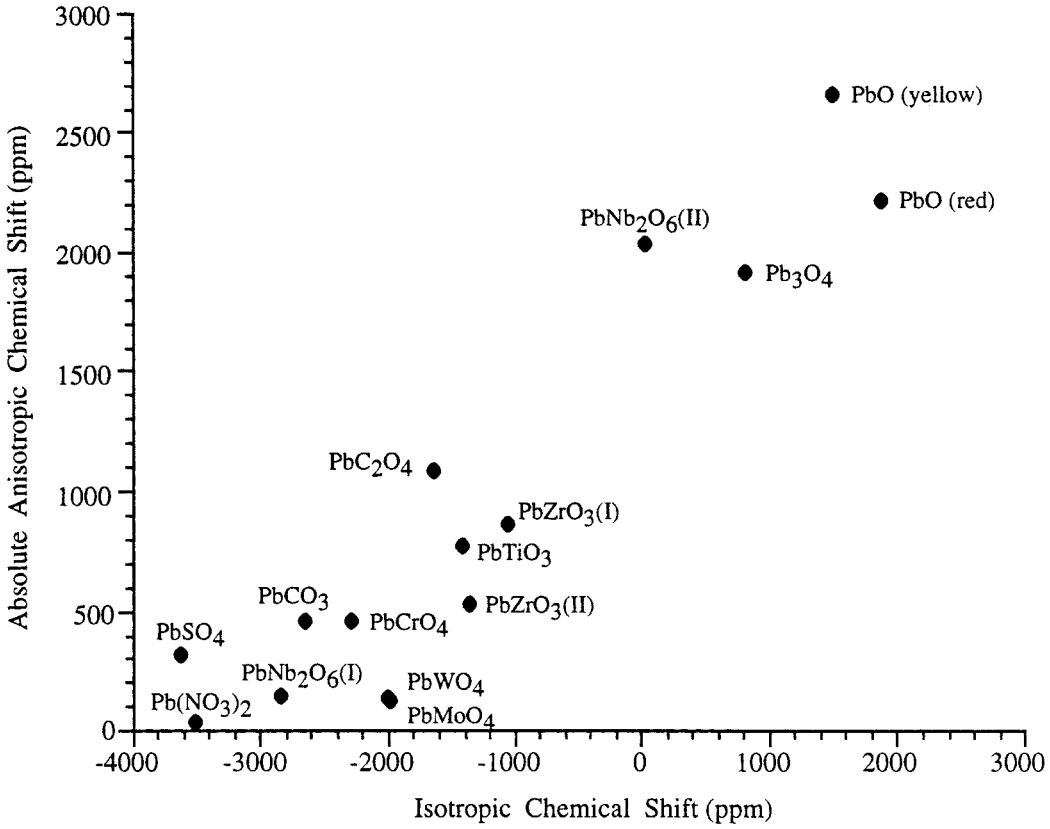

Figure 6. The absolute value of the ^{207}Pb anisotropic chemical shift plotted as a function of ^{207}Pb isotropic chemical shift for Pb(II) sites in a series of lead oxides.

and those reported by Neue et al.[16] and Fayon et al.[18] for Pb(II) sites that have larger absolute anisotropic chemical shifts, possibly due to the different magnetic field strengths and techniques used. For example, our measured anisotropic chemical shift for PbO(red) is larger by 136 ppm than that reported by Fayon et al.,[18] consistent with them not observing the entire spinning sideband manifold.

The full width at half-height of the peaks in the MAS spectra listed in Table 2 indicate the spectral resolution that was obtained. The fwhh of the peaks in the MAS spectra of simple salts ($PbSO_4$, $Pb(NO_3)_2$) is 100 Hz or less, while for compounds that have some covalent character (e.g., $PbTiO_3$, $PbZrO_3$, PbO, Pb_3O_4) the MAS fwhh is between 1.0 and 4.1 kHz. Because MAS averages the orientational dependence of the chemical shift and dipolar interactions, the line widths of ^{207}Pb MAS NMR spectra are due to unresolved scalar coupling (for compounds with multiple lead sites), chemical shift dispersion, and spin−spin relaxation. By comparing the homogeneous line widths ($1/\pi T_2$) determined from the spin−spin relaxation times (T_2) measured for PbO(yellow), PbO(red), and $PbNb_2O_6$ with the full width at half-height of the peaks in the MAS spectra, the homogeneous line width was determined to be a minor contribution to the fwhh for these compounds.

Spin−lattice relaxation is caused by a fluctuating magnetic field at the nucleus, which may result from motion of the local electronic environment. Interestingly, the ^{207}Pb spin−lattice relaxation times (T_1) in the compounds studied vary from about 1 s to more than 160 s and do not appear to be correlated with the presence of a lone pair of electrons nor with any of the chemical shift parameters (δ_{iso}, δ_{aniso}, η).

The absolute value of the anisotropic chemical shift plotted as a function of the isotropic chemical shift for the Pb(II) sites studied appears to be correlated, as shown in Figure 6. Lead(II) sites in ionic materials have relatively symmetric local electronic environments and hence diamagnetically shifted isotropic (−3600 to −2500 ppm) and small anisotropic (<500 ppm) chemical shifts. Covalent Pb−O bonds lead to asymmetric local electronic environments resulting in paramagnetically shifted isotropic and large absolute anisotropic chemical shifts. The compounds that have the most covalent Pb−O bonds (PbO, Pb_3O_4) have the largest isotropic (800 to 1900 ppm) and absolute anisotropic (1900 to 2600 ppm) chemical shifts. While there is not a direct correlation between isotropic and anisotropic chemical shifts, the plot shown in Figure 6 is useful in qualitatively determining the covalency of lead(II) sites and was used to assign the ^{207}Pb NMR resonances of $PbZrO_3$ and $PbNb_2O_6$ to specific crystallographic sites. The isotropic and anisotropic chemical shifts of other heavy ions, with filled electron subshells, such as ^{119}Sn(II) and ^{209}Bi(III), should be similarly related.

Coordination numbers, degree of covalency, the presence of a lone pair of electrons, bond lengths, and bond angles are all factors that influence the symmetry of the electronic environment of lead(II) sites and to some extent are all related. For example, highly covalent Pb−O bonds are often concomitant with the presence of a lone pair of electrons (e.g., PbO, Pb_3O_4).[64] No single structural parameter completely characterizes the local electronic environment nor directly correlates with the ^{207}Pb NMR chemical shift parameters. For example, PbO exists in two polymorphs and the lead(II) sites in each form have four nearest-neighbor oxygen; however, the isotropic chemical shifts are quite different due to the difference in symmetry of the two sites. The two Pb(II) sites in $PbZrO_3$ have the same average Pb−O bond lengths (2.95 Å); however, the isotropic and anisotropic chemical shifts are substantially different. The symmetry of the local electronic environment of Pb(II) ions and

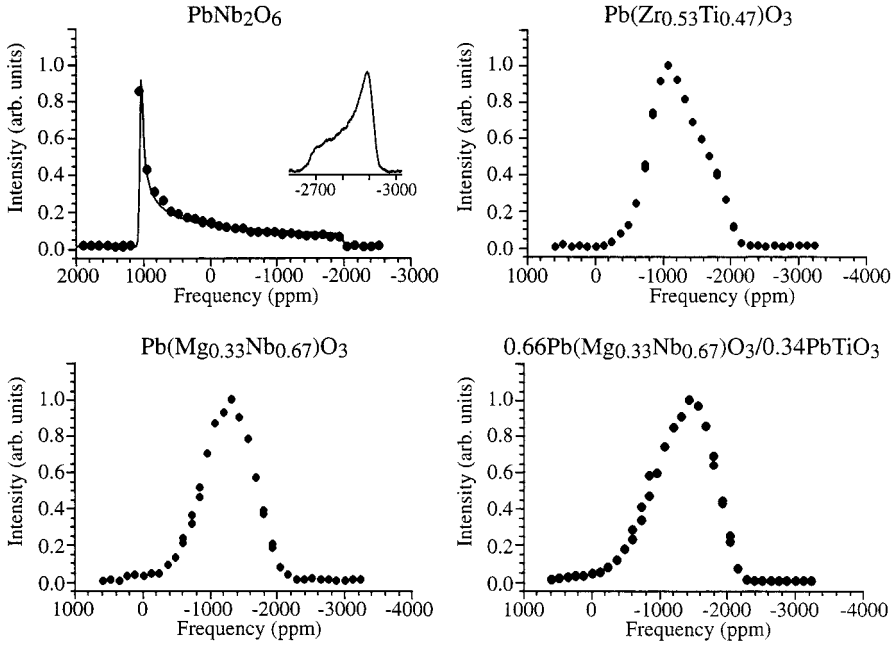

Figure 7. ^{207}Pb NMR spectra of $PbNb_2O_6$, $Pb(Zr_{0.53}Ti_{0.47})O_3$, $Pb(Mg_{0.33}Nb_{0.67})O_3$, and $0.66Pb(Mg_{0.33}Nb_{0.67})O_3/0.34PbTiO_3$ acquired at 9.4 T using the "point-by-point" method (see the Experimental Section for details). The solid points are the measured intensities at each frequency. Only the spectrum of $PbNb_2O_6$ was fit to a simulated line shape (solid line). A ^{207}Pb NMR spectrum of sites 2 and 3 of $PbNb_2O_6$ is shown as an inset above the "point-by-point" spectrum of $PbNb_2O_6$. The ^{207}Pb NMR spectra of $Pb(Zr_{0.53}Ti_{0.47})O_3$, $Pb(Mg_{0.33}Nb_{0.67})O_3$, and $0.66Pb(Mg_{0.33}Nb_{0.67})O_3/0.34PbTiO_3$ have Gaussian-like line shapes with peak maxima at −1090 ppm, −1329 ppm, and −1450 ppm, respectively.

covalency of Pb−O bonds appear to be the best predictors of ^{207}Pb NMR chemical shifts, though they are difficult to characterize quantitatively. The correlation between coordination number and ^{207}Pb isotropic chemical shifts, for coordination numbers greater than seven reported by Fayon et al.[18] is principally a result of sites with higher coordination numbers having electronic environments with higher symmetry.

^{207}Pb NMR Spectroscopy of Lead Niobate and Lead-Based Electronic Materials. ^{207}Pb NMR spectra of lead metaniobate ($PbNb_2O_6$), $Pb(Zr_{0.53}Ti_{0.47})O_3$, $Pb(Mg_{0.33}Nb_{0.67})O_3$ (PMN), and 0.66PMN/0.34PT acquired using the "point-by-point" method are shown in Figure 7. Only the spectrum of $PbNb_2O_6$ was fit to a simulated line shape. While the low-temperature rhombohedral form of $PbNb_2O_6$ studied here is not an electronic material, the complexity of its multiple Pb(II) sites and unique structure provides a test for the utility of ^{207}Pb NMR spectroscopy for the study of complex materials. The niobium(V) ions in $PbNb_2O_6$ are surrounded by six oxygen in a pseudo-octahedral arrangement. These pseudo-octahedra are connected either by sharing opposite corners forming A-type six-member rings or by sharing edges and corners alternatively forming B-type six-member rings as shown in Figure 8.[29] These six-member rings are stacked in the sequence −BBABBABBA− and form tunnel-like holes throughout the lattice. The Pb(II) ions are in the center of the holes between two six-member rings. There are three different Pb(II) sites corresponding to sites between BA, AB, and BB ring-pairs. The Pb(II) site between the BB rings has twelve nearest-neighbor oxygen and three short Pb−O distances of 2.34 Å, and hence is assigned to the broad ^{207}Pb NMR resonance shown in Figure 7 that has a paramagnetically shifted isotropic (134 ppm) and substantial anisotropic (−2024 ppm) chemical shift. The C_3 symmetry axis of this Pb(II) site is consistent with the observed asymmetry parameter of zero ($\eta = 0$) determined from the ^{207}Pb NMR spectrum.

The two Pb(II) sites located between A and B six-member rings have different Pb−O distances according to X-ray diffraction.[29] However, the ^{207}Pb NMR resonances corresponding to these two Pb(II) sites overlap (spectrum shown as an inset in Figure 7), possibly due to motion of the lead(II) ions that is fast on the time scale of the NMR measurements (≈1 ms). The NMR resonance assigned to these two Pb(II) sites has a diamagnetically shifted isotropic chemical shift (−2829 ppm), a relatively small anisotropic chemical shift (149 ppm), and an asymmetry parameter of zero ($\eta = 0$), consistent with their highly symmetric environment and relatively high degree of ionic character as indicated by the relatively long Pb−O distances.

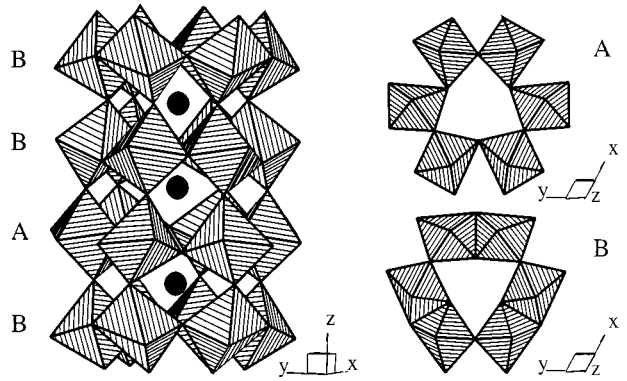

Figure 8. The structure of $PbNb_2O_6$. On the right are the two different types of six-member rings with each pseudo-octahedra corner-shared (A-type, top) or corner-, and edge-shared alternatively (B-type, bottom). These six-member rings are stacked in the order −ABBABB− by sharing the corner of each octahedral unit thus forming tunnel-like holes. The lead(II) sites are in the holes between two six-member rings.

Complex ferroelectric materials with the perovskite lattice structure and the general formula $Pb(B'_xB''_{1-x})O_3$, such as $Pb(Zr_{0.53}Ti_{0.47})O_3$ and $Pb(Mg_{0.33}Nb_{0.67})O_3$ studied here, have two different B-site cations and have electrical properties that are dependent on the local B-site cation ordering. Dielectric perovskites that lack long-range B-site order (random B-site occupancy) with large domain lengths >100 nm, such as lead zirconium titanate ($Pb(Zr_xTi_{1-x})O_3$) in both rhombohedral and

tetragonal phases corresponding to compositions between $Pb(Zr_{0.90}Ti_{0.10})O_3$ and $Pb(Zr_{0.10}Ti_{0.90})O_3$, exhibit normal ferroelectric behavior.[65−68] Structures displaying long-range order, with short domain lengths (2−50 nm), containing partial B-site cation ordering such as in lead magnesium niobate (PMN) are relaxor ferroelectrics, and have broad, diffuse structural phase transitions instead of the sharply defined transition temperatures observed for normal ferroelectrics.

For $Pb(Zr_xTi_{1-x})O_3$, a range of structural phases with different Zr/Ti ratios exist, including cubic, high- and low-temperature rhombohedral, and high- and low-temperature tetragonal phases.[65−68] These materials have random B-site (Zr/Ti) occupancy and exhibit both piezoelectric and electrostrictive properties at the $Pb(Zr_{0.53}Ti_{0.47})O_3$ composition, which is at the morphological phase boundary between the rhombohedral and tetragonal structural phases. Due to the random distribution of zirconium(IV) and titanium(IV) ions among the B-sites, $Pb(Zr_{0.53}Ti_{0.47})O_3$ has not been completely characterized by X-ray or neutron diffraction techniques and the Pb−O distances have not been accurately measured. However, it has been determined that the Pb(II) sites in $Pb(Zr_{0.53}Ti_{0.47})O_3$ have twelve nearest-neighbor oxygen with Pb−O distances ranging from 2.60 to 3.32 Å.[65−68]

The ^{207}Pb NMR spectrum of $Pb(Zr_{0.53}Ti_{0.47})O_3$ is shown in Figure 7. The broad asymmetric peak has a maximum at −1090 ppm and a fwhh of 800 ppm. The observed peak maximum is in the range of the isotropic chemical shifts observed for the end members of the solid solution, $PbTiO_3$ ($\delta_{iso} = -1419$) and $PbZrO_3$ ($\delta_{iso} = -1363$ and -1017) (Figure 5). The spin−lattice relaxation time of $Pb(Zr_{0.53}Ti_{0.47})O_3$ ($T_1 = 7.3$ s) is also close to that observed for $PbTiO_3$ ($T_1 = 7.1$ s) and the two Pb(II) sites in $PbZrO_3$ ($T_1 = 4.2$ and 5.5 s) as shown in Table 2.

The relaxor ferroelectric $Pb(Mg_{0.33}Nb_{0.67})O_3$ (PMN) undergoes a diffuse phase transition with a maximum temperature (T_M) near −15 °C. Addition of lead titanate leads to the formation of solid solutions of the general formula $(1-x)Pb(Mg_{0.33}Nb_{0.67})O_3/xPbTiO_3$ (PMN/PT) and results in an increase in T_M by approximately 5 °C/mol% PT. Compositions containing less PT than the morphotropic phase boundary composition (near 34 mol% PT) have piezoelectric and ferroelectric properties. Materials containing greater than 34 mol% PT are normal ferroelectrics.

PMN has a perovskite lattice structure with an average cubic unit cell symmetry. The Pb(II) ions in PMN are surrounded by twelve oxygen with Pb−O bond lengths ranging from 2.47 to 3.25 Å.[69,70] The Nb(V) and Mg(II) ions are in 6-coordinate BO_6 sites and are present in a 2:1 mole ratio. The partially disordered B-site occupancy (Mg or Nb) in PMN results in a wide distribution of lead(II) sites. The ^{207}Pb NMR spectra of $Pb(Mg_{0.33}Nb_{0.67})O_3$ (PMN) and 0.66PMN/0.34PT are shown in Figure 7. The broad, slightly asymmetric peak in the ^{207}Pb NMR spectrum of PMN has a fwhh of 1000 ppm and a peak maximum of −1400 ppm. The ^{207}Pb NMR spectrum of 0.66PMN/0.34PT has a fwhh of 1200 ppm and a peak maximum at −1500 ppm. The chemical shifts are consistent with an appreciable degree of covalency of the Pb−O bonds in these materials. The relatively short relaxation time of $Pb(Mg_{0.33}Nb_{0.67})O_3$ could be related to the motion of the niobium(V) ions previously reported,[71] fluctuating electric dipoles associated with its piezoelectric properties, or proximity to a structural phase transition.

$Pb(Zr_{0.53}Ti_{0.47})O_3$, PMN, and 0.66PMN/0.34PT all have perovskite lattice structures. The difference in the frequency shifts of the peak maxima of the broad asymmetric ^{207}Pb resonances of these compounds is most likely due to a difference in the covalency of the Pb−O bonds and is consistent with the Pb−O bonds in $Pb(Zr_{0.53},Ti_{0.47})O_3$ being more covalent than those in PMN and 0.66PMN/0.34PT. The line width of the ^{207}Pb NMR resonances for these three important piezoelectric and ferroelectric systems is dominated by chemical shift anisotropy and chemical shift dispersion. The chemical shift anisotropy is due to the distortion of the Pb(II) site environment from cubic symmetry. The chemical shift dispersion is likely due to the distribution of niobium(V) and magnesium(II) ions in PMN and 0.66PMN/0.34PT and of zirconium(IV) and titanium(IV) ions in $Pb(Zr_{0.53}Ti_{0.47})O_3$.

Conclusions

Solid-state ^{207}Pb NMR spectroscopy has the potential to characterize the local lead(II) environment at the atomic-level in complex inorganic materials and can be used to determine structure−property relationships, location and distribution of substituent species, and motion and diffusion of atoms or ions, as well as other technologically important properties. Solid-state ^{207}Pb NMR spectroscopy is an especially useful technique due to its extreme sensitivity to the bonding and structural environment of lead(II) sites as exemplified by its extraordinarily large range of isotropic (−3611 to 1878 ppm) and anisotropic (−2576 to 457 ppm) chemical shifts. The correlation between the degree of covalency of Pb−O bonds, symmetry of the local electronic environment, and ^{207}Pb chemical shift parameters enables solid-state ^{207}Pb NMR spectra to be readily interpreted; and for compounds with multiple lead sites it can aid the assignment of NMR resonances to specific crystallographic sites. In contrast, coordination numbers and average Pb−O bond lengths have been found to be poor indicators of ^{207}Pb chemical shifts. Furthermore, broad ^{207}Pb NMR resonances (>100 kHz) can be measured accurately and efficiently using the "point-by-point" technique described.

Solid-state ^{207}Pb NMR spectroscopy has proven to be a useful tool for characterizing the structural chemistry of lead-based electronic materials. Further development of solid-state NMR techniques and variable temperature measurements will lead to even more detailed information regarding these important materials, their structural heterogeneity and electronic properties, and the mechanism of ferroelectric and piezoelectric behavior at the atomic level.

While ab initio calculations of the chemical shifts of light atoms have become routine, the calculation of the chemical shifts of heavy atoms such as lead is still very challenging, in part due to relativistic effects such as spin−orbit coupling.[4,5,39−41] The ^{207}Pb isotropic and anisotropic chemical shifts reported here would be a good test for calculations that include relativistic effects.[4,5,39−41]

Acknowledgment. This work was supported by a Department of Defense University Research Initiative Support Program (URISP) grant administered by the Office of Naval Research (Grant 0014-96-1-0781). The authors acknowledge the Colorado State University NMR Center and Professor Gary E. Maciel, Director, and Dr. Herman Lock, Manager, for use of the Chemagnetics CMX-200 spectrometer and associated facilities. Mr. Brian Vollmer is acknowledged for writing the NMR simulation software. Helpful discussions with Professor Angel deDios are appreciated.

References and Notes

(1) Gupta, S. M.; Kulkarni, A. R. *Mater. Chem. Phys.* **1994**, *39*, 98−109.

(2) Jona, F.; Shirane, G. *Ferroelectric Crystals*; Dover Publication, Inc: New York, 1993.
(3) Shirane, G.; Hoshino, S.; Suzuki, K. *Phys. Rev.* **1950**, *80*, 1105−1106.
(4) Hota, R. L.; Misra, C. M.; Tripathi, G. S. *Phys. Rev. B* **1992**, *45*, 10783−10786.
(5) Hota, R. L.; Patnaik, R. C.; Tripathi, G. S.; Misra, P. K. *Phys. Rev. B* **1995**, *51*, 7291−7294.
(6) Weinberg, I. *J. Chem. Phys.* **1962**, *28*, 1112−1113.
(7) Hayakawa, H.; Yoko, T.; Sakka, S. *J. Non-Cryst. Solids* **1995**, *183*, 73−84.
(8) Bray, P. J.; Leventhal, M.; Hooper, H. O. *Phys. Chem. Glasses* **1963**, *4*, 47−66.
(9) Reefman, D.; Benschop, F. J. M.; Brom, H. B.; de Groot, R. A.; van Ruitenbeek, J. M. *Physica C* **1992**, *201*, 119−125.
(10) Kohara, T.; Ueda, K.; Takenaka, H.; Kohori, Y.; Oda, Y. *Physica B* **1990**, *165-166*, 1307−1308.
(11) Benschop, F. J. M.; Brom, H. B.; Maaskant, W. J. A. *Physica C* **1992**, *201* (1−2), 109−118.
(12) Benschop, F. J. M.; Brom, H. B.; Zandbergen, H. W.; Cava, R. J. *Physica C* **1994**, *235−240* (Pt. 4), 2527−2528.
(13) Topic, B.; Haeberlen, U.; Blinc, R.; Arend, H. *J. Phys. C: Solid State Phys.* **1986**, *19*, 3925−3932.
(14) Neue, G.; Dybowski, C.; Smith, M. L.; Barich, D. H. *Solid State Nucl. Magn. Reson.* **1994**, *3*, 115−119.
(15) Dybowski, C.; Smith, M. L.; Hepp, M. A.; Gaffney, E. J.; Neue, G.; Perry, D. L. *Appl. Spectrosc.* **1998**, *52*, 426−429.
(16) Neue, G.; Dybowski, C.; Smith, M. L.; Hepp, M. A.; Perry, D. L. *Solid State Nucl. Magn. Reson.* **1996**, *6*, 241−250.
(17) Gabuda, S. P.; Kozlova, S. G.; Terskikh, V. V.; Dybowski, C.; Neue, G.; Perry, D. L. *Chem. Phys. Lett.* **1999**, *305*, 353−358.
(18) Fayon, F.; Farnan, I.; Bessada, C.; Coutures, J.; Massiot, D.; Coutures, J. P. *J. Am. Chem. Soc.* **1997**, *119*, 6837−6843.
(19) Swartz, S. L.; Shrout, T. R.; Schulz, W. A.; Cross, L. E. *J. Am. Ceram. Soc.* **1984**, 311−315.
(20) Bursill, L. A.; Qian, H.; Peng, J.-L.; Fan, Y.-D. *Physica B* **1995**, *216*, 1−23.
(21) Cross, L. E. *Ferroelectrics* **1994**, *151*, 305−320.
(22) Warren, W. L.; Robertson, J.; Dimos, D.; Tuttle, B. A.; Pike, G. E.; Payne, D. A. *Phys. Rev. B* **1996**, *53*, 3080−3087.
(23) The five most intense peaks in the powder X-ray diffraction pattern of $PbNb_2O_6$ (rhombohedral form) were 2θ (rel intensity), 28.71°(100.00), 29.45°(88.93), 51.84°(52.84), 41.62°(40.26), and 56.62°(28.56).
(24) The five most intense peaks in the powder X-ray diffraction pattern of PMN were 2θ (rel intensity), 31.16°(100.00), 55.54°(42.33), 44.70°(32.73), 38.44°(18.55), and 21.86°(15.27).
(25) The five most intense peaks in the powder X-ray diffraction pattern of $Pb(Zr_{0.53}Ti_{0.47})O_3$ (tetragonal form) were 2θ (rel intensity), 31.01°(100.00), 55.14°(41.20), 44.44°(29.48), 38.24°(13.31), and 21.79°(9.47).
(26) The five most intense peaks in the powder X-ray diffraction pattern of 0.66PMN/0.34PT (rhombohedral/tetragonal phase boundary) were 31.42°(100), 56.14°(47.85), 45.24°(35.98), 38.76°(23.73), and 21.12°(17.65).
(27) Dambekalne, M.; Sternberg, A.; Brante, I.; Antonova, M.; Kapenieks, A. *Ferroelectrics* **1986**, *69*, 21−31.
(28) Mahe, R. *Bull. Soc. Chim. Fr.* **1967**, *1967*, 1878−1884.
(29) Francomb, M. H.; Lewis, B. *Acta Crystallogr.* **1958**, *11*, 696−703.
(30) Swartz, S. L.; Shrout, T. R. *Mater. Res. Bull.* **1982**, *17*, 1245−1250.
(31) Grandinetti, P. J. RMN; 1.2 ed.; Department of Chemistry, Ohio State University: Columbus, OH, 1996.
(32) Degroot, H. J. M.; Smith, S. O.; Kolbert, A. C.; Courtin, J. M. L.; Winkel, C.; Lugtenburg, J.; Herzfeld, J.; Griffin, R. G. *J. Magn. Reson.* **1991**, *91*, 30−38.
(33) Herzfeld, J.; Berger, A. E. *J. Chem. Phys.* **1980**, *73*, 6021−6030.
(34) Harris, R. K. *Nuclear Magnetic Resonance Spectroscopy: A Physicochemical View*, 1st ed.; Longman Scientific & Technical: Essex, England, 1986.
(35) Cohen, M. H.; Reif, F. *Solid State Phys.* **1957**, *5*, 321−438.
(36) Andrew, E. R.; Bradbury, A.; Eades, R. G. *Nature* **1958**, *182*, 1659−1659.
(37) Andrew, E. R.; Bradbury, A.; Eades, R. G. *Nature* **1959**, *183*, 1802−1803.
(38) Lowe, I. J. *Phys. Rev. Lett.* **1959**, *2*, 285−287.
(39) Vaara, J.; Ruud, K.; Vahtras, O.; Agren, H.; Jokisaari, J. *J. Chem. Phys.* **1998**, *109*, 1212−1222.
(40) Han, Y.-K.; Bae, C.; Lee, Y. S. *J. Chem. Phys.* **1999**, *110*, 9353−9359.
(41) Fukui, H.; Baba, T. *J. Chem. Phys.* **1998**, *108*, 3854−3862.
(42) Pople, J. A. *Proc. R. Soc. London* **1956**, *A239*, 541−549.
(43) Pople, J. A. *Proc. R. Soc. London* **1956**, *A239*, 550−556.
(44) Ramsey, N. F. *Phys. Rev.* **1950**, *78*, 699−703.
(45) Ramsey, N. F. *Phys. Rev.* **1952**, *86*, 243−246.
(46) Slichter, C. P. *Principles of Magnetic Resonance*; Springer-Verlag: Berlin, Germany, 1990.
(47) Orgel, L. E. *Mol. Phys.* **1958**, *1*, 322−325.
(48) Bondi, A. *J. Phys. Chem.* **1964**, *68*, 441−451.
(49) Shannon, R. D.; Prewitt, C. T. *Acta Crystallogr.* **1970**, *B26*, 1046.
(50) Wells, A. F. *Structural Inorganic Chemistry*; Clarendon Press: Oxford, England, 1975.
(51) Nowotny, H.; Heger, G. *Acta Crystallogr. C* **1983**, *485*, 133−135.
(52) Wyckoff, R. W. G. *Crystal Structures*, 2nd ed.; J. Wiley & Sons: New York, 1965; Vol. 3.
(53) Kakegawa, K.; Wakabayashi, T.; Sasaki, Y. *J. Mater. Sci. Lett.* **1988**, *7*, 230−232.
(54) Christensen, A. N.; Cox, D. E.; Lehmann, M. S. Ø. *Acta Chem. Scand.* **1989**, *43*, 19−25.
(55) Wyckoff, R. W. G. *Crystal Structures*, 2nd ed.; J. Wiley & Sons: New York, 1965; Vol. 1.
(56) Gavarri, J.; Weigel, D. *J. Solid State Chem.* **1975**, *13*, 252−257.
(57) Wyckoff, R. W. G. *Crystal Structures*, 2nd ed.; J. Wiley & Sons: New York, 1965; Vol. 2.
(58) Shirane, G.; Pepinsky, R.; Frazer, B. C. *Acta Crystallogr.* **1956**, *9*, 131−140.
(59) Jona, F.; Shirane, G.; Mazzi, F.; Pepensky, R. *Phys. Rev.* **1957**, *105*, 849−856.
(60) Megaw, H. D. *Proc. Phys. Soc. London* **1946**, *58*, 133−152.
(61) Sawaguchi, E.; Meniwa, H.; Hoshino, S. *Phys. Rev.* **1951**, *83*, 1078−1080.
(62) Nolle, A. *Z. Naturforsch* **1977**, *32a*, 964−967.
(63) Lauterbur, P. C.; Burke, J. J. *J. Chem. Phys.* **1965**, *42*, 439−440.
(64) Bargar, J. R.; Brown, G. E.; Parks, G. A. *Geochim. Cosmochim. Acta* **1997**, *61*, 2617−2637.
(65) Jirak, Z.; Kala, T. *Ferroelectrics* **1988**, *82*, 79−84.
(66) Ito, H.; Shiozaki, Y.; Sawaguchi, E. *J. Phys. Soc. Jpn.* **1983**, *52*, 913−919.
(67) Michel, C.; Moreau, J. M.; Achenbach, G. D.; Gerson, R.; James, W. J. *Solid State Comm.* **1969**, *7*, 865−868.
(68) Sawaguchi, E. *J. Phys. Soc. Jpn.* **1953**, *8*, 615−629.
(69) Verbaere, A.; Piffard, Y.; Ye, Z. G.; Husson, E. *Mater. Res. Bull.* **1992**, *27*, 1227−1234.
(70) de Mathan, N.; Husson, E.; Calvarin, G.; Gavarri, J. R.; Hewat, A. N.; Morell, A. *J. Phys.: Condens. Mater.* **1991**, *3*, 8159−8171.
(71) Glinchuk, M. D.; Bykov, I. P.; Laguta, V. V. *Ferroelectrics* **1993**, *143*, 39−47.
(72) Brody, S. B. *J. Chem. Phys.* **1942**, *10*, 650−652.